International Journal of Recent Technology and Engineering (IJRTE)
ISSN: 2277-3878, Volume-8 Issue-4, November 2019

Deconvolution for Enhancement of Biological Images Obtained by Fluorescence Microscopy

Reetoja Nag, Raunak Kumar Das

Abstract: ***Intricate details of cells and tissues can be visualised by fluorescence microscopy and the images obtained can be then be quantitatively analysed. However, during image acquisition, distortions of the images occur by convolving the object with Point Spread Function. To remove this blurring, computational deconvolution methods are used in which the original image is restored with improved contrast. Our study analysed various fluorescence images, after the nuclei segmentation of the images, by both Deblurring (Blind Deconvolution, Lucy Richardson and Wiener filtering) and Restoration algorithms (Inverse filtering and Regularised filtering), which are the two main categories of deconvolution methods, in MATLAB 2016b. After statistical analysis (Mann Whitney U test) of area and homogeneity of the segmented nuclei of the various images for the different deconvolution methods, statistical significant difference was found in the case of area ((p=0.027) for Original vs. Inverse filter and (p=0.029) for Original vs. Regularised filter)) for restoration algorithms and for homogeneity, it was found for original vs. all the deconvolution methods, which shows that quantitative evaluation of the features can be used to further determine the better deconvolution method and in this case Restoration algorithms proves better than Deblurring algorithms.***

Index Terms**: *Deconvolution, Deblurring algorithms, Fluorescence microscopy, Point Spread Function, Restoration algorithms***

I. INTRODUCTION

In research related to biomedical field, analysis and quantitative measurement in the structures of biological tissues and cells (e.g. total amount of DNA inside a cell nucleus), interactions and dynamics of cellular forces can be investigated by fluorescence microscopic imaging [1]. Fluorescence microscopy can be used as a quantitative imaging assay and the introduction of green fluorescent protein and its spectral variants is responsible for it. However, the nature of the imaging acquisition system and its response to known standards should be validated and the relative signal levels in different parts of the image acquired should be preserved by any image processing algorithm used for analysis of quantitative imaging assays [2]. The quantitative analysis of samples is hampered by problems in imaging system which leads to the reduction of maximal resolution obtainable by it leading to measurement defects which in turn disfigure the image. Thus the imaging hardware, the acquisition process, fundamental aspects of photon detection must be taken into contemplation [3]. The distortion or blurring acquired in the image are restored using image processing algorithm known as image deconvolution [4]. It is also used to enhance contrast and perceive small, faint objects in the image that might be unnoticed otherwise. The two major types of deconvolution methods are deblurring and restoration algorithms. Though the deblurring algorithms remove blur, mishandling of blurred light occurs by treating a series of optical sections as individual two-dimensional entities [5]. On the other hand, restoration algorithms convolve object with point spread function of the microscope to produce image data [6]. Deconvolution of fluorescence microscopy biological images by means of computational restoration procedures has engrossed attention in the past couple of years [5], [6].

A. Structure and function of fluorescence microscopy systems

Fluorescence microscopes use the in addition to or instead of reflection and absorption, the event of fluorescence and phosphorescence. The two major divisions of these light microscopes are Widefield and Confocal, which are used extensively (Figure 1). 3-D data from the sample is documented in a set of 2-D images of various in-focus planes of the sample. In case of Widefield microscope, images have low lateral resolution since image at the detector plane contains both in-focus plane and out-of-focus knowledge as light released from the out-of-focus regions cannot be differentiated from the in-focus plane light [7]. On the other hand, Confocal microscopic images have high lateral resolution as much of the out-of-focus light is averted by introducing a pinhole in front of the detector. However low Signal to Noise ratio is obtained in this case as only those photons passing through the pinhole are gathered [7]. Different types of systemic noise needs to be minimised by pre-processing the digital image data before quantitative analysis.

Manuscript published on November 30, 2019.
* Correspondence Author
Reetoja Nag*, PhD student, Centre for Biomaterials, Cellular and Molecular Theranostics, Vellore Institute of Technology,Vellore-632014,Tamil Nadu, India. Email :reetoja.nag2016@vitstudent.ac.in
Raunak Kumar Das, Assisitant Professor, Centre for Biomaterials, Cellular and Molecular Theranostics, Vellore Institute of Technology,Vellore-632014,Tamil Nadu, India. Email: raunakkumardas@vit.ac.in

In one example, illumination variation across the area of charged couple device (CCD) camera used in fluorescence microscopy especially in Widefield microscopy is improved by correcting the flat field of CCD field thus leading it to not being affected by illumination systemic errors [8]. In another example, time dependent illumination variation is corrected by simply summing the fluorescence signal in each frame and then fitting the summed signals to a polynomial in the fluorescence microscopy [9].

The quantitative relationship of the image data ideally should be preserved before using any processing algorithm as this will help interpretation of identified objects [10].

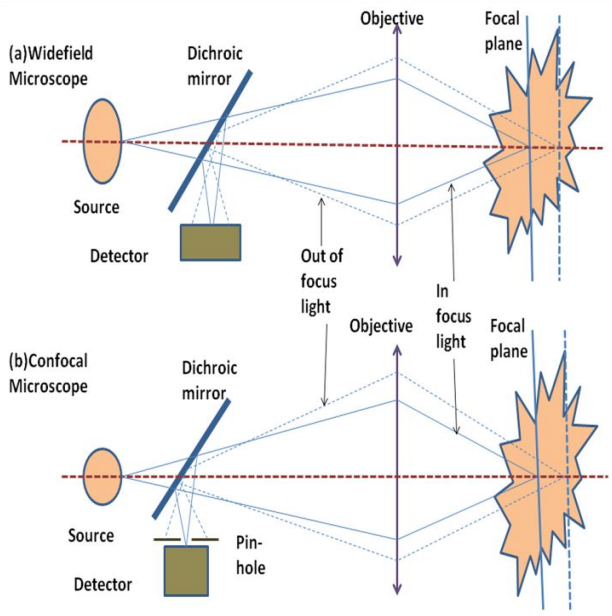

Figure 1: Structure of the two different types of fluorescence microscopes(A)Widefield Microscope (B)Confocal Microscope

B. Deconvolution techniques in fluorescence microscopy

In fluorescence microscopy, during imaging of cells and tissues, objective lens with high numerical aperture and good resolving power are used in order to decrease photon shot noise and to identify small objects respectively. However these lenses have narrow depth of field which results in an image that combines in-focus as well as out-focus information from focal plane and elsewhere of the sample respectively which results in decrease in contrast and not resolving of individual objects. This is a problem mostly in imaging in cases of intrinsically thick tissue and cells as density of the blurred light amplifies linearly along with the thickness of the sample. Hence in samples which are more than 10–20 mm thick, blurring becomes an eminent problem [11]. The blurring produced on a sample by an objective lens is expressed by the point-spread function (PSF). Methods related to PSF have been extensively reviewed till date [12]-[17]. Blurring in fluorescence microscopy is caused by convolution of the object with the PSF in addition to noise and deconvolution reinstates the original object to an enhanced resolution and higher SNR level. The procedure is illustrated in Figure 2 where ⊗ represents the convolution operation. Deconvolution method in fluorescence microscopic systems comprises of optical and computational techniques [18]. In optical method, the out-of-focus light is cast off before it reaches the detector in order to decrease distortion. This results in distinct but anisotropic image which has to be improved by computational methods. In computational technique, from each optical slice of a 2-D data, out of-focus contribution is deducted by the computer. For deconvolution involving medical imaging application, computational speed as well as dependability of the solution is vital [18].

C. Models and properties of microscopic PSF

The distortion or blurring in 3-D image of the specimen, obtained by focusing the fluorescence microscope at different planes of the structure of series of 2-D images of the sample, is caused by mostly out-of-focus light which amounts to the characterization of PSF i.e. the fluorescence microscopic system's 3-D impulse response [19],[20]. Due to introduction of diffraction ring patterns in radial planes by finite lens aperture by fluorescence microscope, a microscopic PSF shows radial directional symmetry and optical directional asymmetry resulting in low resolution of the acquired 3-D sample, mostly due to band limited PSF [21]. During image acquisition process, the corruption during image measurement is caused by intrinsic and extrinsic noise. Intrinsic noise follows Poisson model where an arbitrary number of light photons is created after each photon hits the detector screen. Extrinsic noise is established by other sources which are exemplified by assorted statistics like Gaussian, uniform etc. [22].In case of fluorescence microscopy, negligible extrinsic noise is produced due to use of CCD camera as image detector. Gaussian noise model is preferred over Poisson noise model, which is more realistic in comparison, as it simplifies numerical computation [23].

The Gaussian noise model is given by-

$$g(x, y, z) = f(x, y, z) \otimes h(x, y, z) + w(x, y, z),\ x, y, z \in R \quad (1)$$

where f(x, y, z) is the 3-D specimen of interest, h(x, y, z) is the PSF of the fluorescence microscope and w(x, y, z) is an additive Gaussian noise and ⊗ represents the convolution operation. The matrix form of (1) is

$$g = Hf + w \quad (2)$$

where H is the sampled PSF, and f is the vector form of the discrete object w is the 3-D vector form of w(x, y, z) [7].

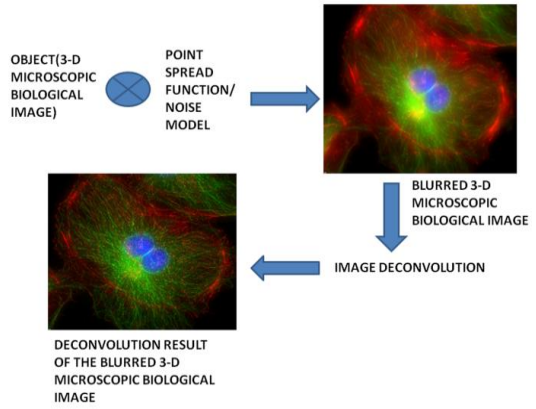

Figure 2:Process of convolution and deconvolution of an image obtained by fluorescence microscopy(Pictures taken as an example from online site of Biological Department Imaging Facility, Washington University in St.Louis.)

http://www.biology.wustl.edu/imaging-facility/specs-deltavision.php

Before starting the deconvolution operation, the background term can be eliminated from the obtained image after its estimation, hence it is not included in the model. However Gaussian model can outperform Poisson model only in the case of high SNR [24].

In our study, we have compared different deconvolution image processing methods, both deblurring and restoration, on the nuclei of biological cells of various fluorescence microscopic images, convolved with Gaussian Noise Model, in order to determine the deconvolution method most suitable for giving clearer resolution and subsequent information of fluorescence microscopic biological images.

II. METHODOLOGY

A. Segmentation of nuclei of the cells in fluorescence microscopic biological images

10 human cell images were taken from the online Cell Imaging Library, maintained by Centre for Research in Biological Systems. The following images were taken-CIL:10102 (Cultured retinal pigment epithelial cells immunofluorescently labelled for clathrin (green) and nucleus (blue)), CIL:10103 (Cultured retinal pigment epithelial cells immunofluorescently labelled for adaptor protein-2 (AP2) (green) and nucleus (blue)),CIL:10104(Cultured retinal pigment epithelial cells immunofluorescently labelled for transferrin receptor (TfnR) (green) and nucleus (blue)), CIL:13382(Cultured retinal pigment epithelial cells immunofluorescently labelled for transferrin receptor (TfnR) (green) and nucleus (blue)),CIL:13383(The nucleolus during mammary epithelial differentiation and early mammary tumorigenesis. Proliferating 3D cultures of MCF-10.B2 cells treated to activate ErbB2 were stained at day 20 with ANA-N antibody to detect nucleoli (green) and counterstained with DAPI to delineate nuclei (blue)),CIL:13384(FISH detection of PTEN and VEGF gene loci in MCF-10.B2 cells during mammary epithelial differentiation and early mammary tumorigenesis. PTEN (red) and VEGF (green) were detected in paraformaldehyde fixed MCF10A.B2 cells grown for 20 days under 3D growth conditions. DAPI (blue) delineates nuclei), CIL: 13385(FISH detection of PTEN and VEGF gene loci in MCF-10.B2 cells during mammary epithelial differentiation and early mammary tumorigenesis. PTEN (red) and VEGF (green) were detected in paraformaldehyde fixed MCF10A.B2 cells grown for 20 days under 3D growth conditions with 10 days of constitutive activation of ErbB2. DAPI (blue) delineates nuclei),CIL:35158(Live mitotic HeLa cell treated with epsin1 siRNA, DiOC6(3)to label mitotic membranes (green), and Hoechst 33258 to label chromosomes in the nuclei(blue)),CIL:35161(Live mitotic HeLa cell treated with control siRNA, DiOC6(3)to label mitotic membranes (green), and Hoechst 33258 to label chromosomes in the nuclei (blue))and CIL:41066(Fluorescent micrograph of A549 cells (adenocarcinomic human alveolar basal epithelial cells) showing the nucleus (blue) and mRNAs of TFRC (transferrin receptor) identified by fluorescently labelled oligonucleotide).

The RGB images were split into Red, Green and Blue channels in MATLAB 2016b and the blue channelled images were selected as they represented nuclei.

B. Deconvolution image processing methods

Deconvolution on the images was done by both deblurring and restoration algorithms. In deblurring, Wiener, Lucy Richardson and Blind deconvolution filtering were used. In restoration, Inverse and Regularised filters were used. For all the methods, Gaussian model was used as PSF. The methods were carried out in MATLAB 2016b.The general characteristics of the deconvolution methods carried out over the years, for fluorescence microscopy images are given in Table I.

1) Deblurring algorithms

In deblurring algorithms, also known as neighbour based methods, the contribution of out-of-focus fluorescence in each optical section is recognized and eliminated by first taking into consideration the image as a sum of the in-focus signal and the out-of focus signal from neighbouring sections and deblurring one section at a time. A given optical section and its immediate neighbours are given as-

$$\text{image}_n = \text{object}_n \otimes \text{psf}_n + \text{object}_{n+1} \otimes \text{psf}_{n+1} + \text{object}_{n-1} \otimes \text{psf}_{n-1} \quad (3)$$

To calculate object n, by replacing with suitable optical sections in the image data, equation (3) can be rewritten as-

$$\text{image}_n = \text{object}_n \otimes \text{psf}_n + \text{image}_{n+1} \otimes \text{psf}_{n+1} + \text{image}_{n-1} \otimes \text{psf}_{n-1} \quad (4)$$

The advantage of using deblurring algorithms is that the can be computed quickly in spite of the neighbours in the solution adding errors [25].

a) Wiener filtering

The image deformation model shown in (1) is for additive Gaussian noise which is independent of signal. g(x, y, z), for a known h(x, y, z), in (1) is deconvolved as-

$$\hat{f}(x, y, z) = g(x, y, z) \otimes \hat{h}(x, y, z) \quad (5)$$

where $x, y, z \in R$ and $\hat{h}(x, y, z)$ is the mean-square error (MSE) i.e. optimal stationary linear filter for the deconvolution [7].

b) Blind Deconvolution and Lucy Richardson methods

Most algorithms rely on precise PSF modelling, which poses its own set of problems like present noise in an experimentally measured PSF and inability to remove all aberrations of microscopic optics by theoretical PSF. The advantage of blind deconvolution lies in the fact that it can determine both microscopic PSF and 3-D image simultaneously [26].The Blind deconvolution is based on Lucy Richardson algorithm which can be given as-

$$\hat{f}_{i+1}(\alpha) = \{ h(\beta,\alpha)g(\beta)d\beta / h(\beta,\gamma)\hat{f}_i(\gamma)d\gamma \} \hat{f}_i(\alpha) \quad (6)$$

where α and β are two events, $\hat{f}i(\alpha)$ is the object distribution at the *i* th iteration, h (β, α) is the PSF centred at α, and the degraded image is g (β).

Extending the problem to 3-D, equation (6) in its Blind Deconvolution form can be rewritten as-

$$\hat{f}^k_{i+1}(x, y, z) = \{[g(x, y, z)/ \hat{f}^k_i(x, y, z) \otimes \hat{h}^{k-1}(x, y, z)]\} \otimes \hat{h}^{k-1}(-x,-y,-z)\} \hat{f}^k_i(x, y, z) \quad (7)$$

where at the *k*th blind iteration it is assumed that the PSF is known from the *(k - 1)* th iteration.

The object $f^{k}(x, y, z)$ is calculated for a specified number of Lucy Richardson iterations as in (7), where the index *i* represents Lucy Richardson iteration. The PSF $h^{k}(x, y, z)$ is then calculated from (7) for the same number of Lucy Richardson iterations [7].

Table I: Characteristics of Deconvolution Methods carried out of over the years on 3-D Fluorescence Microscopy Images

S. No	Deconvolution Method	Algorithms	PSF Model	Characteristics
1.	Deblurring	Wiener filter	Gaussian	High frequency components suppressed and ringing artefacts established in resultant image [28-30].
		Blind deconvolution and Lucy-Richardson	Poisson and Gaussian	Computationally exhaustive, lots of parameters involved [31-33].
2.	Restoration	Inverse filter	Poisson and Gaussian	Noise intensified, uncomplicated and computationally speedy [34,35].
		Regularised filter	Gaussian	Uncomplicated and computationally speedy, signal to noise ratio reduced and structural artefacts established in resultant image [36,37].

In order to lessen the noise sensitivity present in Lucy Richardson algorithm, image recorded is convolved with Gaussian function to repress the high-frequency parts/low SNR regions .Further, same Gaussian is convolve d with PSF to cause smoothing of Lucy- Richardson algorithm [27].

2) Restoration algorithms

Restoration algorithms are another method for deconvolution of microscopic images. After the object is estimated by equation (8), it is convolved with PSF to produce the image data given by equation (9).

$$\text{image} = \text{object} \otimes \text{psf} \quad (8)$$

$$\text{image} = \hat{o} \otimes \text{psf} \quad (9)$$

where $\hat{o}$ represents an approximation at the object. These methods are iterative and advance through the following steps:

1. $\hat{i}^{(k)} = \hat{o}^{(k)} \otimes \text{psf}$
2. $\hat{o}^{(k+1)} = \hat{o}^{(k)}\ \text{image}/\ \hat{i}^{(k)}$
3. If $\hat{o}^{(k+1)} < 0$, then $\hat{o}^{(k+1)} = 0$
4. k=k+1;

where $\hat{i}$ is the estimate after blurring with the psf and k represents iteration number [25].

In step 1,the estimate of the object $\hat{o}(k)$ is convolved with psf to give estimate blur $\hat{i}(k)$.In step 2,new estimate $\hat{o}(k+1)$ is produced after updating old estimate $\hat{o}(k)$ by comparing blur $\hat{i}(k)$ with image data. In step 3, any values of $\hat{o}(k+1)$ which are less than 0, are approximated as 0.This step is done to avoid linearity. In step 4, the iteration is amplified so that until a stable $\hat{o}(k+1)$ is achieved, steps are repeated from step 1 [25].

a) Inverse filtering

Assuming the Gaussian noise model given in (1) without the additive Gaussian noise, the 3-D deconvolved image for inverse filtering method, for a known h(x, y, z), is given by the following equation-

$$\hat{f}(x, y, z) = F^{-1}(G(\omega_x, \omega y, \omega z))/(H(\omega_x, \omega y, \omega z)\}) \quad (10)$$

where ω_x, ω_y, and ω_z denote the frequency domain counterparts of the space variables x, y, and z, respectively; $G(\omega_x,\omega_y,\omega_z)$ and $H(\omega_x,\omega_y,\omega_z)$ are the 3-D Fourier transforms of g(x, y, z) and h(x, y, z); $\hat{f}(x, y, z)$ is the deconvolved image of the specimen in 3-D; and F^{-1} is the inverse Fourier transform operation in 3-D [7].

b) Regularised filtering

Regularised filter or least square method follows the image deformation model given by the following equation-

$$g(x, y, z) = f(x, y, z) \otimes h(x, y, z)\ x, y, z \in R \quad (11)$$

The matrix form of equation (11) is given by the following equation -

$$g = Hf \quad (12)$$

The least square solution of equation (12) is given by the following equation-

$$\hat{f} = (H^{T}H)^{-1}H^{T}g \quad (13)$$

where $\hat{f}$ denotes the estimated 3-D image in vector form after the deconvolution operation [7].

C. Feature extraction and statistical analysis

After deconvolution on the nuclei of the 10 images were done by Wiener, Lucy-Richardson, Blind deconvolution, Inverse and Regularised filtering, features like area and homogeneity of the nuclei were extracted in MATLAB 2016b and statistical analysis(Mann Whitney U test) was done on the values obtained to determine statistical significant difference between the different deconvolution processes (Table II).

III. RESULTS AND DISCUSSION

The original images i.e. CIL:10102, CIL:10103, CIL:10104, CIL:13382, CIL:13383, CIL:13384, CIL:13385 ,CIL:35158,CIL:35161 and CIL:41066 are shown in Figures 3(A), 3(B), 3(C), 3(D), 3(E), 3(F), 3(G), 3(H), 3(I) and 3(J) respectively.

The result of deconvolution methods i.e. Wiener, Blind Deconvolution, Lucy Richardson, Inverse filter and Regularised filter on the segmented nuclei of the image CIL:10102 are shown in Figures 4(B), 4(C), 4(D), 4(E) and 4(F) respectively, of the image CIL:10103 are shown in Figures 5(B), 5(C), 5(D), 5(E) and 5(F) respectively, of the image CIL:10104 is shown in Figures 6(B), 6(C), 6(D), 6(E) and 6(F) respectively, of the image CIL:13382 is shown in Figures 7(B), 7(C), 7(D), 7(E) and 7(F) respectively, of the image CIL:13383 is shown in Figures 8(B), 8(C), 8(D), 8(E) and 8(F) respectively, of the image CIL:13384 is shown in Figures 9(B), 9(C), 9(D), 9(E) and 9(F) respectively, of the image CIL:13385 is shown in Figures 10(B), 10(C), 10(D), 10(E) and 10(F) respectively, of the image CIL:35158 is shown in Figures 11(B), 11(C), 11(D), 11(E) and 11(F) respectively, of the image CIL:35161 is shown in Figures 12(B), 12(C), 12(D), 12(E) and 12(F) respectively and of the image CIL:41066 is shown in Figures 13(B), 13(C), 13(D), 13(E) and 13(F) respectively.

Deconvolution algorithms are mostly done to decrease blur and progress contrast in an image. Estimation and removal of blur is done in the case of deblurring algorithms(Blind Deconvolution, Lucy-Richardson and Wiener filter).Restoration algorithms(Inverse and Regularised filter),on the other hand, somewhat reinstate the blurred signal to it's in focus position by first producing an approximation of the object, thus using the blurred signal as the in-focus signal. This allows for improved SNR, intensities in the image being preserved and better contrast in images.

After statistical analysis (Mann Whitney U test) on the values of area and homogeneity for different deconvolution methods on the segmented nuclei of the fluorescence microscopic images (Table II), we obtained statistical significant differences between Original image vs. Inverse filtered image (p=0.027) and Original image vs. Regularised filtered image (p=0.029) i.e. the restoration deconvolution methods in case of area. In case of homogeneity, statistical significant difference was obtained between Original image vs. Blind Deconvolution filtered image (p=0.00068), Original image vs. Inverse filtered image (p=0.00008), Original images. Lucy-Richardson filtered image (p=0.0006), Original image vs. Regularised filtered image (p=0.003) and Original image vs. Wiener filtered image (p<0.00001) i.e. for all deconvolution methods.

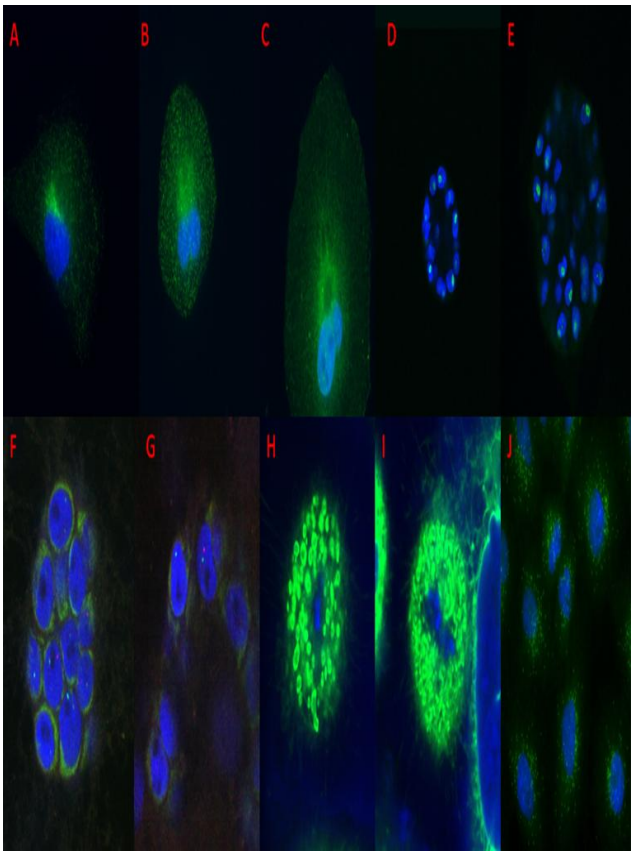

Figure 3.Original images(A) CIL:10102 (B)CIL:10103 (C) CIL:10104 (D)CIL:13382 (E)CIL:13383(F)CIL:13384 (G) CIL:13385 (H)CIL:35158(I)CIL:35161 (J)CIL:41066

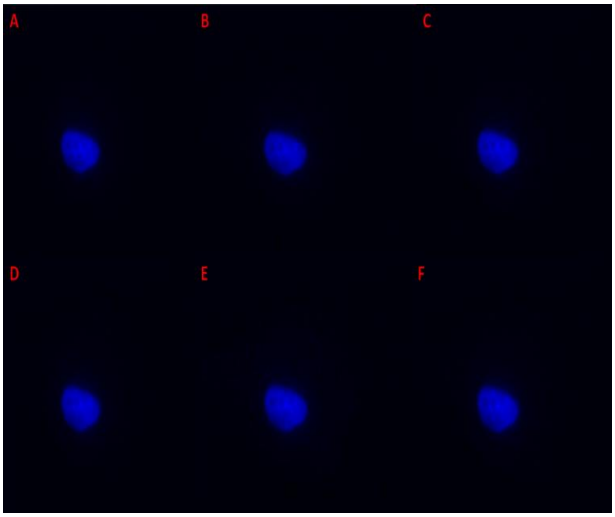

Figure 4(A) Segmented nuclei of image of CIL:10102 (B)Deconvolution by Weiner filter on 4(A) (C) Deconvolution by Blind Deconvolution on 4(A) (D) Deconvolution by Lucy Richardson on 4(A) (E) Deconvolution by Inverse filter on 4(A) (F) Deconvolution by Regularised filter on 4(A)

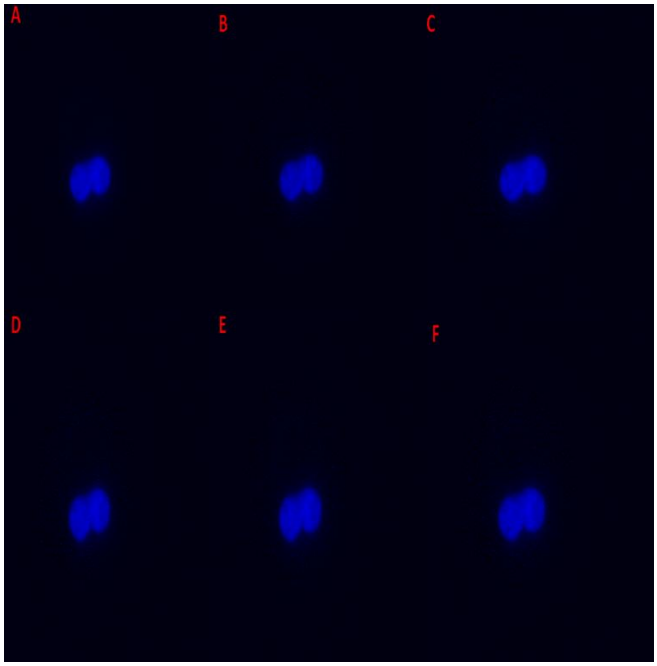

Figure 5(A) Segmented nuclei of image of CIL:10103 (B)Deconvolution by Weiner filter on 5(A) (C) Deconvolution by Blind Deconvolution on 5(A) (D) Deconvolution by Lucy Richardson on 5(A) (E) Deconvolution by Inverse filter on 5(A) (F) Deconvolution by Regularised filter on 5(A)

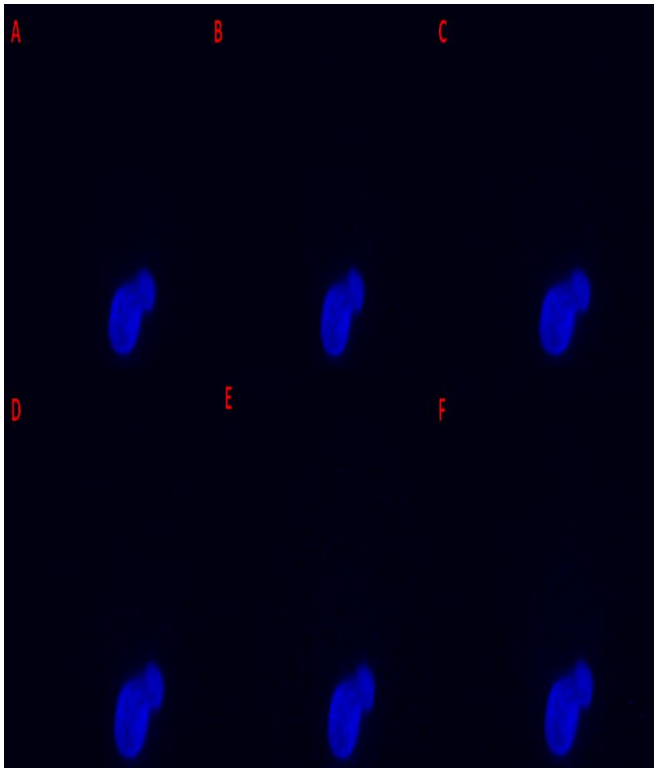

Figure 6(A) Segmented nuclei of image of CIL:10104

(B)Deconvolution by Weiner filter on 6(A) (C) Deconvolution by Blind Deconvolution on 6(A) (D) Deconvolution by Lucy Richardson on 6(A) (E) Deconvolution by Inverse filter on 6(A) (F) Deconvolution by Regularised filter on 6(A)

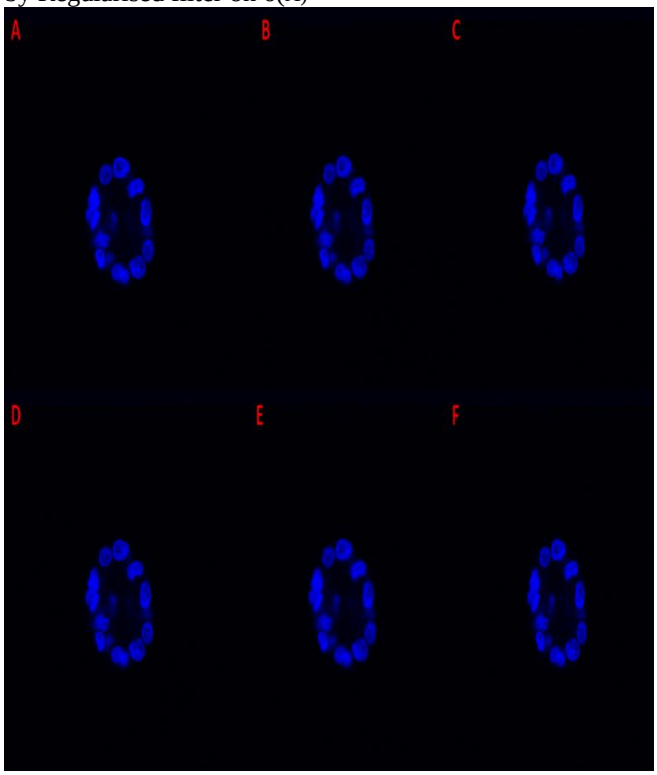

Figure 7(A) Segmented nuclei of image of CIL:13382

(B)Deconvolution by Weiner filter on 7(A) (C) Deconvolution by Blind Deconvolution on 7(A) (D) Deconvolution by Lucy Richardson on 7(A) (E) Deconvolution by Inverse filter on 7(A) (F) Deconvolution by Regularised filter on 7(A)

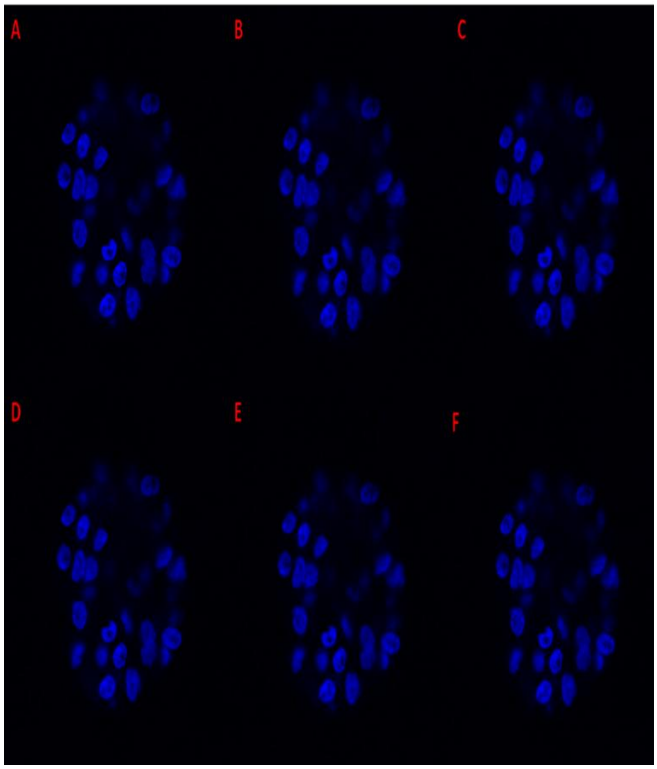

Figure 8(A) Segmented nuclei of image of CIL:13383
(B)Deconvolution by Weiner filter on 8(A) (C) Deconvolution by Blind Deconvolution on 8(A) (D) Deconvolution by Lucy Richardson on 8(A) (E) Deconvolution by Inverse filter on 8(A) (F) Deconvolution by Regularised filter on 8(A)

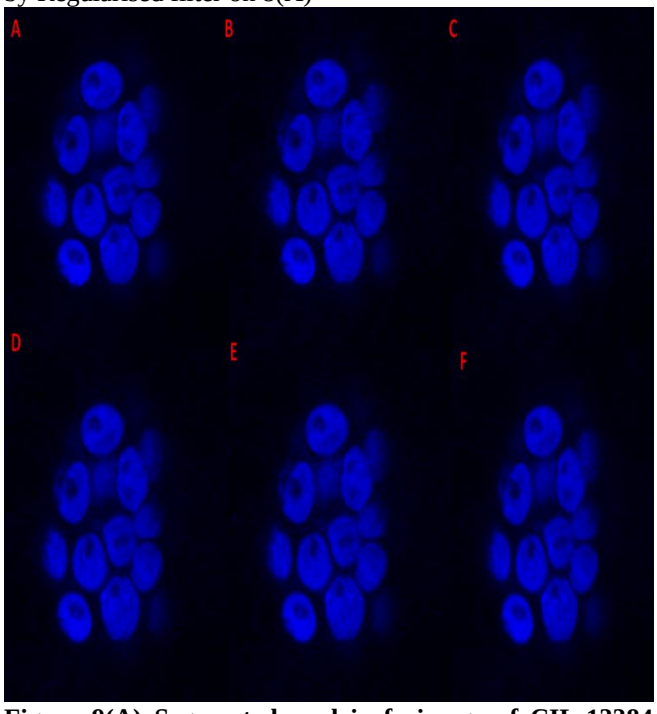

Figure 9(A) Segmented nuclei of image of CIL:13384
(B)Deconvolution by Weiner filter on 9(A) (C) Deconvolution by Blind Deconvolution on 9(A) (D) Deconvolution by Lucy Richardson on 9(A) (E) Deconvolution by Inverse filter on 9(A) (F) Deconvolution by Regularised filter on 9(A)

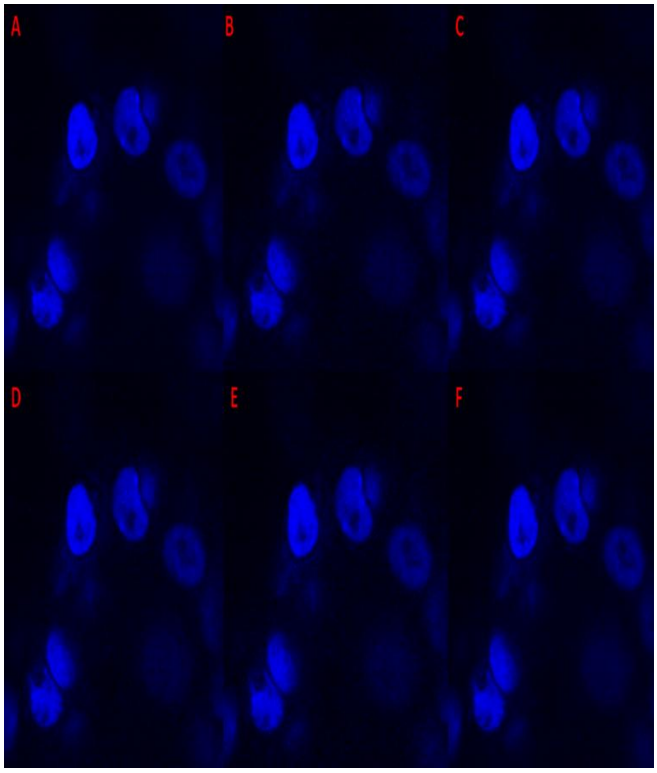

Figure 10(A) Segmented nuclei of image of CIL:13385 (B)Deconvolution by Weiner filter on 10(A) (C) Deconvolution by Blind Deconvolution on 10(A) (D) Deconvolution by Lucy Richardson on 10(A) (E) Deconvolution by Inverse filter on 10(A) (F) Deconvolution by Regularised filter on 10(A)

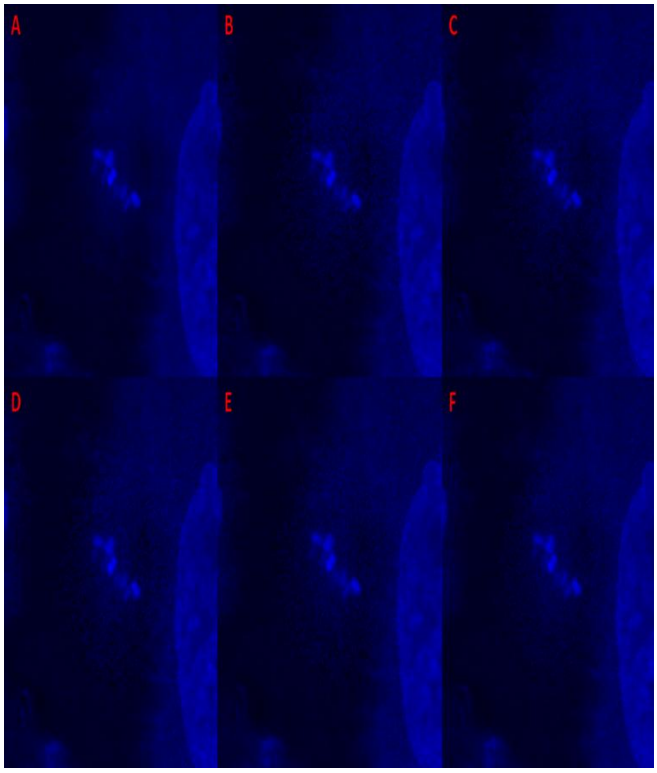

Figure 12(A) Segmented nuclei of image of CIL:35161 (B)Deconvolution by Weiner filter on 12(A) (C) Deconvolution by Blind Deconvolution on 12(A) (D) Deconvolution by Lucy Richardson on 12(A) (E) Deconvolution by Inverse filter on 12(A) (F) Deconvolution by Regularised filter on 12(A)

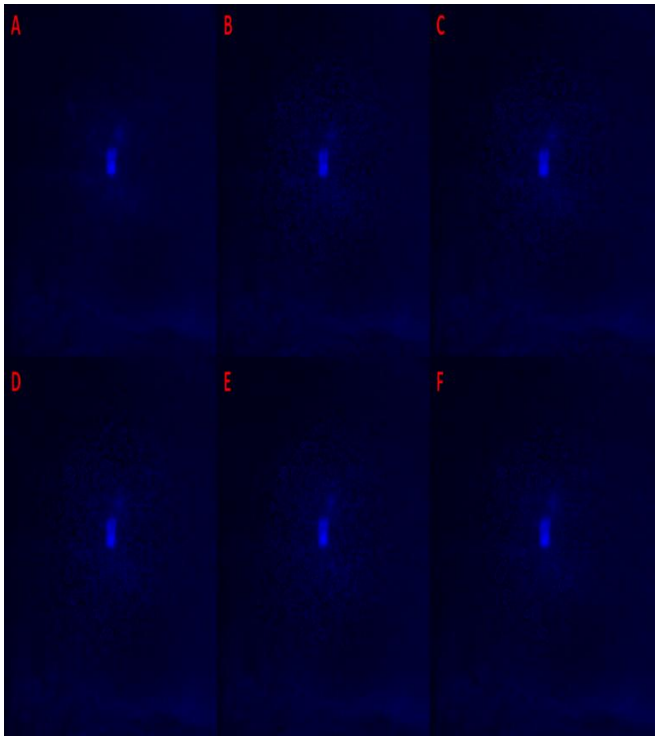

Figure 11(A) Segmented nuclei of image of CIL:35158 (B)Deconvolution by Weiner filter on 11(A) (C) Deconvolution by Blind Deconvolution on 11(A) (D) Deconvolution by Lucy Richardson on 11(A) (E) Deconvolution by Inverse filter on 11(A) (F) Deconvolution by Regularised filter on 11(A)

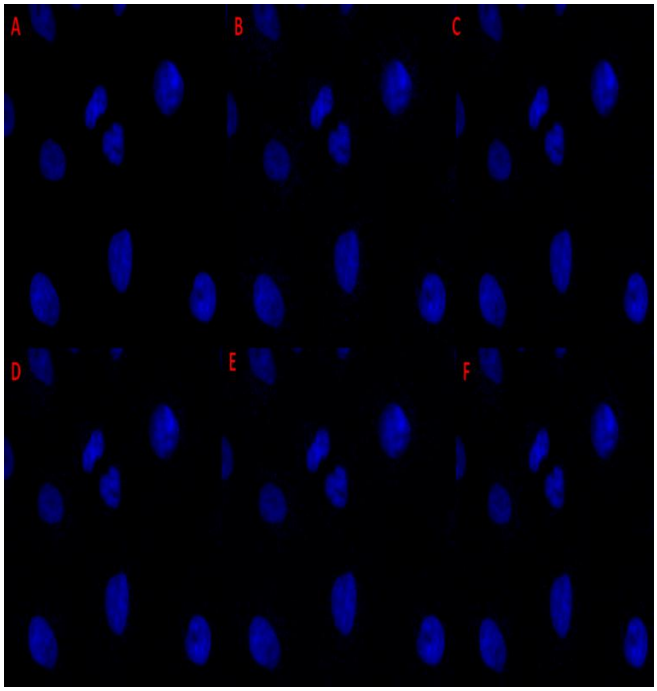

Figure 13(A) Segmented nuclei of image of CIL:41066(B)Deconvolution by Weiner filter on 13(A) (C) Deconvolution by Blind Deconvolution on 13(A) (D) Deconvolution by Lucy Richardson on 13(A) (E) Deconvolution by Inverse filter on 13(A) (F) Deconvolution by Regularised filter on 13(A)

Table II: Analysis by Mann Whitney U test on features of the segmented nuclei on fluorescence microscopic biological images for different deconvolution method

Feature	Original	Blind Deconvolution	Inverse	Lucy-Richardson	Regularised	Wiener	Mann Whitney U test	*p* values
Area	1068.015±1541.79	1269.77±1251.2	1316.49±1290.01	1272.83±1271.17	1378.149±1293.51	1303.91±1290.21	Original vs. Blind Deconvolution	0.051
							Original vs. Inverse	0.027
							Original vs. Lucy-Richardson	0.058
							Original vs. Regularised	0.029
							Original vs. Wiener	0.051
Homogeneity	0.8272±0.0783	0.7791±0.0904	0.7666±0.0945	0.7818±0.0836	0.7837±0.0906	0.7732±0.0746	Original vs. Blind Deconvolution	0.00068
							Original vs. Inverse	0.00008
							Original vs. Lucy-Richardson	0.0006
							Original vs. Regularised	0.003
							Original vs. Wiener	<0.00001

IV. CONCLUSION AND FUTURE WORK

Our study tries to compare the effect of different deconvolution methods (deblurring and restoration algorithms) on various fluorescence biological images. On visual inspection, it was found that restoration algorithms i.e. Inverse filtering and Regularised Filtering gave better clearer and better contrast in the images, in some cases deblurring algorithm like Wiener filter also gave improved results in comparison to other methods. Statistical significant differences were also found for original image vs. restoration algorithms((p=0.027) for Original vs. Inverse filter and (p=0.029) for Original vs. Regularised filter) in case of extracted feature area of the segmented nuclei and for homogeneity of the segmented nuclei of the images, statistical significant difference was found between original images vs. all the deconvolution methods.

So, overall deconvolution methods, especially restoration algorithms can improve the contrast and give clearer images which has been blurred or distorted during image acquisition for fluorescence biological microscopic images and quantitative and analysis of the features like area and homogeneity can also give a better comparison between the deconvolution methods. The hardware necessities for these calculations i.e. brisk CPUs and important memory requirements are now customarily obtainable in desktop computers, so deconvolution can be easily done by biologists and microscopists.

In future, larger datasets can be used and statistical analysis on more number of features of the images can be done to get improvised validated results.

ACKNOWLEDGMENT

The authors would like to thank the online Cell Imaging Library from where the biological images were taken for computational analysis and Vellore Institute of Technology for providing institutional support.

REFERENCES

1. Carlavan, Mikael, and Laure Blanc-Féraud. "Sparse Poisson noisy image deblurring." IEEE Transactions on Image Processing 21, no. 4 (2012): 1834-1846. https://doi.org/10.1109/TIP.2011.2175934
2. Rödiger, Stefan, Peter Schierack, Alexander Böhm, Jörg Nitschke, Ingo Berger, Ulrike Frömmel, Carsten Schmidt et al. "A highly versatile microscope imaging technology platform for the multiplex real-time detection of biomolecules and autoimmune antibodies." In Molecular diagnostics, pp. 35-74. Springer, Berlin, Heidelberg, 2012. https://doi.org/10.1007/10_2011_132.
3. Beck, Amir, and Marc Teboulle. "A fast iterative shrinkage-thresholding algorithm for linear inverse problems." SIAM journal on imaging sciences 2, no. 1 (2009): 183-202. https://doi.org/10.1137/080716542
4. Huisken, Jan, and Didier YR Stainier. "Selective plane illumination microscopy techniques in developmental biology." Development 136, no. 12 (2009): 1963-1975. https://doi.org/10.1242/dev.022426
5. Prevedel, Robert, Young-Gyu Yoon, Maximilian Hoffmann, Nikita Pak, Gordon Wetzstein, Saul Kato, Tina Schrödel et al. "Simultaneous whole-animal 3D imaging of neuronal activity using light-field microscopy." Nature methods 11, no. 7 (2014): 727. https://doi.org/10.1038/nmeth.2964
6. Biggs, David SC. "3D deconvolution microscopy." Current Protocols in Cytometry 52, no. 1 (2010): 12-19. https://doi.org/10.1002/0471142956.cy1219s52
7. Sarder, Pinaki, and Arye Nehorai. "Deconvolution methods for 3-D fluorescence microscopy images." IEEE Signal Processing Magazine 23, no. 3 (2006): 32-45. https://doi.org/10.1109/MSP.2006.1628876
8. Bertero, Mario, Patrizia Boccacci, Gabriele Desiderà, and G. Vicidomini. "Image deblurring with Poisson data: from cells to galaxies." Inverse Problems 25, no. 12 (2009): 123006. https://doi.org/10.1088/0266-5611/25/12/123006
9. Dupé, François-Xavier, Jalal M. Fadili, and Jean-Luc Starck. "A proximal iteration for deconvolving Poisson noisy images using sparse representations." IEEE Transactions on Image Processing 18, no. 2 (2009): 310-321. https://doi.org/10.1109/TIP.2008.2008223
10. Dobigeon, Nicolas, Alfred O. Hero, and Jean-Yves Tourneret. "Hierarchical Bayesian sparse image reconstruction with application to MRFM." IEEE transactions on Image Processing 18, no. 9 (2009): 2059-2070. https://doi.org/10.1109/TIP.2009.2024067
11. Vonesch, Cédric, François Aguet, J-L. Vonesch, and Michael Unser. "The colored revolution of bioimaging." IEEE signal processing magazine 23, no. 3 (2006): 20-31. https://doi.org/10.1109/MSP.2006.1628875

12. Maalouf, Elie, Bruno Colicchio, and Alain Dieterlen. "Fluorescence microscopy three-dimensional depth variant point spread function interpolation using Zernike moments." JOSA A 28, no. 9 (2011): 1864-1870. https://doi.org/10.1364/JOSAA.28.001864
13. Quirin, Sean, Sri Rama Prasanna Pavani, and Rafael Piestun. "Optimal 3D single-molecule localization for superresolution microscopy with aberrations and engineered point spread functions." Proceedings of the National Academy of Sciences 109, no. 3 (2012): 675-679. https://doi.org/10.1073/pnas.1109011108
14. Kner, Peter, John W. Sedat, David A. Agard, and Zvi Kam. "High-resolution wide-field microscopy with adaptive optics for spherical aberration correction and motionless focusing." Journal of microscopy 237, no. 2 (2010): 136-147. https://doi.org/10.1111/j.1365-2818.2009.03315.x
15. Chen, Yuzhang, Min Xia, Wei Li, Xiaohui Zhang, and Kecheng Yang. "Comparison of point spread models for underwater image restoration." Optik-International Journal for Light and Electron Optics 123, no. 9 (2012): 753-757. https://doi.org/10.1016/j.ijleo.2011.06.010
16. Yuan, Shuai, and Chrysanthe Preza. "Point-spread function engineering to reduce the impact of spherical aberration on 3D computational fluorescence microscopy imaging." Optics Express 19, no. 23 (2011): 23298-23314. https://doi.org/10.1364/OE.19.023298
17. Arigovindan, Muthuvel, Joshua Shaevitz, John McGowan, John W. Sedat, and David A. Agard. "A Parallel Product-Convolution approach for representing depth varying Point Spread Functions in 3D widefield microscopy based on principal component analysis." Optics express 18, no. 7 (2010): 6461-6476. https://doi.org/10.1364/OE.18.006461
18. Sibarita, Jean-Baptiste. "Deconvolution microscopy." In Microscopy Techniques, pp. 201-243. Springer, Berlin, Heidelberg, 2005. https://doi.org/10.1007/b102215
19. Toomre, Derek, and Joerg Bewersdorf. "A new wave of cellular imaging." Annual review of cell and developmental biology 26 (2010): 285-314.https://doi.org/10.1146/annurev-cellbio-100109-104048
20. Juette, Manuel F., Travis J. Gould, Mark D. Lessard, Michael J. Mlodzianoski, Bhupendra S. Nagpure, Brian T. Bennett, Samuel T. Hess, and Joerg Bewersdorf. "Three-dimensional sub–100 nm resolution fluorescence microscopy of thick samples." Nature methods 5, no. 6 (2008): 527. https://doi.org/10.1038/nmeth.1211
21. Gardini, Lucia, Marco Capitanio, and Francesco S. Pavone. "3D tracking of single nanoparticles and quantum dots in living cells by out-of-focus imaging with diffraction pattern recognition." Scientific reports 5 (2015): 16088. https://doi.org/10.1038/srep16088
22. Luisier, Florian, Thierry Blu, and Michael Unser. "Image denoising in mixed Poisson–Gaussian noise." IEEE Transactions on image processing 20, no. 3 (2011): 696-708. https://doi.org/10.1109/TIP.2010.2073477
23. Jezierska, Anna, Hugues Talbot, Caroline Chaux, Jean-Christophe Pesquet, and Gilbert Engler. "Poisson-Gaussian noise parameter estimation in fluorescence microscopy imaging." In 2012 9th IEEE International Symposium on Biomedical Imaging (ISBI), pp. 1663-1666. IEEE, 2012. https://doi.org/10.1109/ISBI.2012.6235897
24. Boulanger, Jérôme, Charles Kervrann, Patrick Bouthemy, Peter Elbau, Jean-Baptiste Sibarita, and Jean Salamero. "Patch-based nonlocal functional for denoising fluorescence microscopy image sequences." IEEE transactions on medical imaging 29, no. 2 (2010): 442-454. https://doi.org/10.1109/TMI.2009.2033991
25. Swedlow, Jason R. "Quantitative fluorescence microscopy and image deconvolution." In Methods in cell biology, vol. 114, pp. 407-426. Academic Press, 2013. https://doi.org/10.1016/B978-0-12-407761-4.00017-8
26. Jiang, Ming, and Ge Wang. "Development of blind image deconvolution and its applications." Journal of X-ray Science and Technology 11, no. 1 (2003): 13-19.
27. Singh, Manoj Kumar, Uma Shanker Tiwary, and Young-Hoon Kim. "An adaptively accelerated Lucy-Richardson method for image deblurring." EURASIP Journal on Advances in Signal Processing 2008 (2008): 52. https://doi.org/10.1155/2008/365021
28. Benesty, Jacob, Jingdong Chen, Yiteng Arden Huang, and Simon Doclo. "Study of the Wiener filter for noise reduction." In Speech Enhancement, pp. 9-41. Springer, Berlin, Heidelberg, 2005. https://doi.org/10.1007/3-540-27489-8_2
29. Chen, Jingdong, Jacob Benesty, Yiteng Huang, and Simon Doclo. "New insights into the noise reduction Wiener filter." IEEE Transactions on audio, speech, and language processing 14, no. 4 (2006): 1218-1234. https://doi.org/10.1109/TSA.2005.860851
30. Tai, Yu-Wing, and Stephen Lin. "Motion-aware noise filtering for deblurring of noisy and blurry images." In 2012 IEEE Conference on Computer Vision and Pattern Recognition, pp. 17-24. IEEE, 2012. https://doi.org/10.1109/CVPR.2012.6247653
31. Dey, Nicolas, Laure Blanc-Feraud, Christophe Zimmer, Pascal Roux, Zvi Kam, Jean-Christophe Olivo-Marin, and Josiane Zerubia. "Richardson–Lucy algorithm with total variation regularization for 3D confocal microscope deconvolution." Microscopy research and technique 69, no. 4 (2006): 260-266. https://doi.org/10.1002/jemt.20294
32. Molina, Rafael, Javier Mateos, and Aggelos K. Katsaggelos. "Blind deconvolution using a variational approach to parameter, image, and blur estimation." IEEE Transactions on Image Processing 15, no. 12 (2006): 3715-3727. https://doi.org/10.1109/TIP.2006.881972
33. Campisi, Patrizio, and Karen Egiazarian, eds. Blind image deconvolution: theory and applications. CRC press, 2016.
34. Li, Jizhou, Feng Xue, and Thierry Blu. "Accurate 3D PSF estimation from a wide-field microscopy image." In 2018 IEEE 15th International Symposium on Biomedical Imaging (ISBI 2018), pp. 501-504. IEEE, 2018.https://doi.org/10.1109/ISBI.2018.8363625
35. Kervrann, Charles, Carlos Óscar Sánchez Sorzano, Scott T. Acton, Jean-Christophe Olivo-Marin, and Michael Unser. "A guided tour of selected image processing and analysis methods for fluorescence and electron microscopy." IEEE Journal of Selected Topics in Signal Processing 10, no. 1 (2016): 6-30. https://doi.org/10.1109/JSTSP.2015.2505402
36. Li, Jizhou, Feng Xue, and Thierry Blu. "Fast and accurate three-dimensional point spread function computation for fluorescence microscopy." JOSA A 34, no. 6 (2017): 1029-1034. https://doi.org/10.1364/JOSAA.34.001029
37. Li, Jizhou, Florian Luisier, and Thierry Blu. "PURE-LET deconvolution of 3D fluorescence microscopy images." In 2017 IEEE 14th International Symposium on Biomedical Imaging (ISBI 2017), pp. 723-727. IEEE, 2017. https://doi.org/10.1109/ISBI.2017.7950621